Effect of Seed Power on the Inter-Modal Four-Wave-Mixing Effect in Distributed Side-Pumped Fiber Amplifiers

Yuan Tian, Jianqiu Cao, Heng Chen, Aimin Liu, Zhiyong Pan, Zhihe Huang, and Jinbao Chen

***Abstract*—The effect of seed power on the inter-modal four-wave mixing (IM-FWM) effect in a distributed side-pumped fiber amplifier is investigated for the first time, to the best of our knowledge. By using a seed source smaller than 70 W, the effect of seed power on the IM-FWM is studied experimentally. Surprisingly, it is found that the IM-FWM effect becomes stronger with the weaker seed. To analyze the physics behind this result, a numerical model is introduced, and the numerical results are in good agreement with the experimental observations. It is revealed that the IM-FWM enhancement is induced by the gain competition between the signal light and the anti-Stokes light of the IM-FWM. It is also found that there is an optimized seed power for suppressing the IM-FWM effect. The experimental and numerical results which are presented in this work can provide significant guidance for understanding the IM-FWM in fiber lasers and amplifiers.**

***Index Terms*—Inter-modal four-wave mixing, mode competition, Yb-doped fiber amplifiers.**

I. Introduction

DUE to their broad applications in industry, medicine, and material processing, among others, high-power Yb-doped fiber lasers have attracted a lot of research attention. In the last two decades, the output power of Yb-doped fiber lasers has increased rapidly [1]–[10] and the milestone of 10-kW output power, with near diffraction-limit beam quality, was achieved in 2009 by the IPG Corporation [5], [11]. However, as power increases, nonlinear effects, such as stimulated Raman scattering (SRS), self-phase modulation (SPM), and four wave-mixing (FWM), become more and more important [12]–[15]. Recently, the inter-modal four-wave mixing (IM-FWM) effect has attracted much attention. IM-FWM is a nonlinear effect inducing energy transfer between various transverse modes. Therefore, it can be induced both in few- and multi-mode fibers [16]–[19]. In fact, the IM-FWM, in high-power fiber lasers, has been observed in experiments and reported in the literature [20]–[22], but with no detailed study given. In 2018, [23] carried out the preliminary theoretical and experimental studies and revealed that the IM-FWM can be suppressed by reducing the coiling diameter in high-power fiber lasers. The phase matching theory was also introduced in detail in [23]. However, this theory can only predict the wavelength of transverse modes produced by IM-FWM but cannot describe the evolutions of these modes in the fiber amplifier.

In this paper, the IM-FWM effect in the distributed side-pumped fiber amplifier is studied. The distributed-pumped fiber amplifier, generally consists no-less-than two sub-amplifiers, has been numerically studied in 2004 and was considered as a promising architecture for high-power applications due to its advantages with respect to thermal management and power scalability [24]–[25]. However, limited by the difficulty in the pump power coupling, the corresponding experimental studies were very few. Recently, however, the development of side-pumped active fiber, allowed for such experimental studies to become feasible and nowadays, with the distributed side-pumped architecture, multi-kW fiber lasers and amplifiers have been created [26]–[29]. The coiling effect on the suppression of IM-FWM was also experimentally investigated in [28].

The IM-FWM can also be observed in the measured spectra reported in our previous work [29], where also showed that the IM-FWM threshold should be related to the seed power. However, in [29] we only studied the SRS, because, to the best of our knowledge, there was no proper numerical model able to be used to study the effect of IM-FWM in the fiber amplifier. In this paper, we present a numerical model for studying the IM-FWM effect in a distributed side-pumped fiber amplifier. This, in turn, will allow the study of the effect that the seed power has on the IM-FWM which will provide significant guidance for understanding the IM-FWM in fiber lasers and amplifiers.

The paper is organized as follows. In Section II, we review the experimental setup and the data found in [29], which will be employed to analyze the power variations of the Stokes and anti-Stokes light of IM-FWM with the seed power. In Section III, a theoretical analysis, based on the phase-matching condition of IM-FWM, is provided to reveal the transverse modes inducing the IM-FWM. The numerical model is introduced in Section IV

Manuscript received February 27, 2022; revised April 29, 2022; accepted May 15, 2022. Date of publication May 26, 2022; date of current version June 7, 2022. This work was supported by the National Natural Science Foundation of China under Grant U20B2058. *(Yuan Tian and Jianqiu Cao are co-first authors and contributed equally to this work.) (Corresponding authors: Jianqiu Cao; Jinbao Chen.)*

The authors are with the College for Advanced Interdisciplinary Studies, National University of Defense Technology, Changsha 410073, China, with the Hunan Provincial Collaborative Innovation Center of High-Power Fiber Laser, Changsha 410073, China, and also with the Hunan Provincial Key Laboratory of High Energy Laser Technology, Changsha 410073, China (e-mail: 610209866@qq.com; jq_cao@126.com; chenheng_nudt@qq.com; 17673122794@163.com; panzy168@163.com; hzhihe@163.com; kdchenjinbao@aliyun.com).

Digital Object Identifier 10.1109/JPHOT.2022.3176495

This work is licensed under a Creative Commons Attribution 4.0 License. For more information, see https://creativecommons.org/licenses/by/4.0/

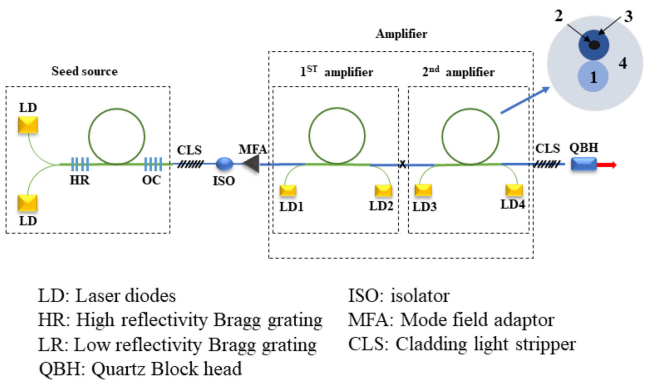

Fig. 1. The schematic of the all-fiber distributed side-pumped fiber laser [29]; The fiber cross section is shown as the inset.

TABLE I
PARAMETERS OF THE FIBER AMPLIFIER

Parameters	Value
Fiber length in each stage (m)	15
Diameters of core 1 (μm)	250
Diameters of core 2 (μm)	25
Diameters of inner-cladding 3 (μm)	250
Diameters of outer-cladding 4 (μm)	650
NA of core 2	0.065
Signal wavelength (nm)	1080
Pump wavelength (nm)	976
Seed beam quality	M^2<1.1

and the underlying physical mechanism is numerically investigated in Section V. Our conclusions are discussed in Section VI.

II. EXPERIMENTAL SETUP AND RESULTS

Although our experimental observations reported in [29] indicate that the seed power influences the IM-FWM effect, no discussion or study has been done, according to our knowledge. In this section, we will study and analyze these experimental observations in the view of IM-FWM effect.

Fig. 1 depicts the experimental setup used. The distributed side-pumped fiber amplifier consists of two sub-amplifiers. In each sub-amplifier, the distributed side-coupled cladding-pumped (DSCCP) fiber (also known as GTWave fiber [30]–[31], multi-clad fiber [32], and multi-element first cladding fiber [33]) is used as the active fiber. The DSCCP fiber consists of one pump fiber and one signal fiber. The pump light is injected into the core (i.e., Core 1) of the pump fiber, and is coupled gradually into the inner cladding (i.e., Cladding 3) of the signal fiber. Then, the lasing can be produced in the active core (i.e., Core 2). The parameters of the DSCCP fiber are given in Table I. The bi-directional pumping scheme is utilized in the fiber amplifier and the pump light is provided by 976-nm wavelength-stabilized laser diodes (WSLDs).

An all-fiber oscillator, fabricated with the 10/130 μm core/cladding-diameter double-cladding ytterbium-doped fiber (DCYF), is utilized to provide the seed light at around 1080 nm. The numerical aperture (NA) of active core is around 0.07 and thus the DCYF should be single mode around 1080 nm. A pair of fiber Bragg gratings (FBG) with the reflectivity of 99% (HR) and 11% (OC) were utilized as cavity reflectors, and their reflection spectra are centered around 1080 nm with 3-dB bandwidth at 2 nm and 1 nm, respectively. The pump light is provided by two 976 nm WSLDs. The seed light, which is provided by the all-fiber oscillator, is injected into the distributed side-pumped fiber amplifier via the cladding light stripper (CLS), the isolator (ISO), and the mode field adaptor (MFA). This seed source configuration provides about 70-W of seed light which can be produced with a beam quality (M2 factor) around 1.08. Then, the output light after the two-stage sub-amplifiers and a CLS is measured through a QBH (Quartz Block Head).

The spectrum variation with respect to the output power, and under various seed powers, is shown in Fig. 2. To illustrate more efficiently the spectral variation, more detailed experimental data, compared to [29], are provided. It can be clearly seen that, two more side lobes, located around 1058 nm and 1102 nm, emerge when the output power is large enough. This, in turn, means that the IM-FWM effect should be present, according to the analysis in Refs. [28]. In this work, a more detailed analysis, based on the phase-matching condition, is presented in Section III. Comparing Fig. 2(a)–(f), it can be found that the IM-FWM threshold (i.e., the output power corresponding to the emergence of IM-FWM) varies with the seed power.

To show the enhancement of IM-FWM more clearly, the powers of 1102 nm Stokes and 1058 nm anti-Stokes light are estimated by spectrum integration and are shown in Fig. 3(a). It can be found that for each seed power, the Stokes and anti-Stokes powers are very close to each other. Apart from that, it is also found that the Stokes power is generally larger than the anti-Stokes counterpart when the seed power is smaller than 36 W. On the other hand, it becomes a little smaller compared to the anti-Stokes power when the seed power is larger than 60 W. A similar conclusion can be also drawn from Fig. 2 by comparing the peak values of two side lobes in each spectrum, i.e., the 1102 nm Stokes power is larger when the seed power is smaller than 36 W.

To understand the phenomenon, we re-examine these spectra in Fig. 2, where it is clear that when the seed power is smaller than 36 W, the strong SRS component is present [see Fig. 2(a)–(c)]. Furthermore, Fig. 2(a)–(c) indicate that with the increment of pump power, the spectral profiles of the SRS and Stokes light gradually join with each other, which means that the Stokes light can be affected by the Raman gain. It is the shown that the relatively larger 1102 nm Stokes power (with respect to the 1058 nm anti-Stokes, with the smaller seed power) should be induced by the broadband Raman gain. This explanation can be verified by Fig. 2(e) and (f) where no SRS is observed. It is found that the 1102 nm Stokes power is not larger compared to the anti-Stokes one without SRS. In fact, Fig. 2 depicts that the SRS can only affect the Stokes light of IM-FWM when it is strong enough. From Fig. 2, it can be found that the SRS becomes stronger

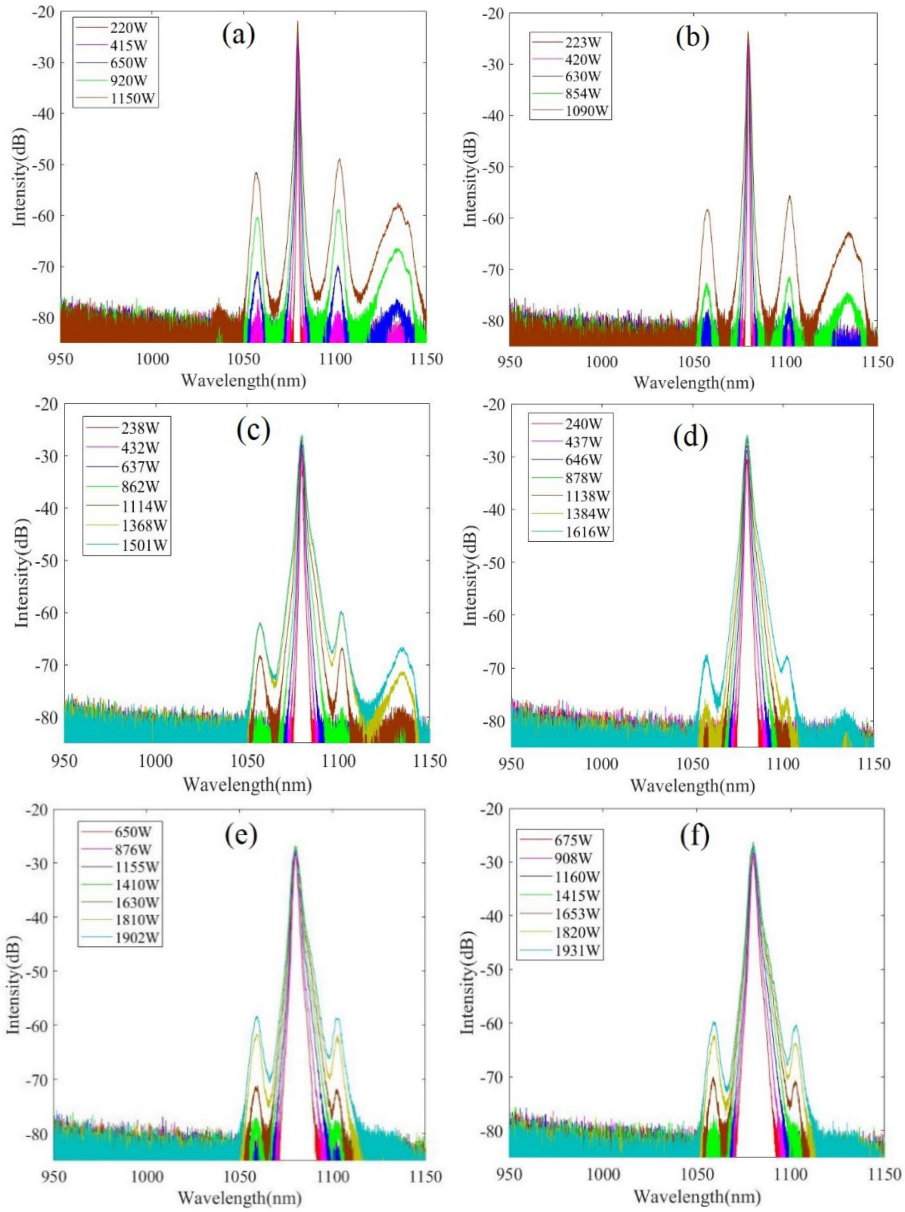

Fig. 2. Output spectrum versus output power under different various seed power; seed power: (a) 10 W; (b) 18 W; (c) 28 W; (d) 36 W; (e) 60 W; (f) 70 W (some data are the same as [29]).

with smaller seed power, a phenomenon known under the term "Weak-seed induced enhancement of SRS" which has been fully investigated in [29].

Fig. 3(b) depicts the total output power as a function of the pump power under different seed powers. It can be found that the output power increase linearly with the pump power, and the seed power has no obvious effect on the slope efficiency which is about 54%. Besides, the increment of output power with the seed power is still so weak that it should not be the origin of the variation of IM-FWM threshold shown in Fig. 3(a).

III. Phase-Matching Analysis of IM-FWM

To perform the numerical study, it is important to determine the transverse modes involved in the IM-FWM effect. Therefore, in this section, we will employ a method based on the phase-matching condition [23], [34], described by,

$$\kappa = \Delta k_M + \Delta\, k_W = \Delta\omega^2\chi + \beta(\omega_1) + \beta(\omega_4) - \beta(\omega_2) - \beta(\omega_3) = 0 \quad (1)$$

In (1), κ is the phase mismatch. Δk_M and Δk_W describe the mismatches caused by the material dispersion and waveguide dispersion, respectively. χ is the dispersion parameter and for a wavelength of 1080 nm its value is 15.293 fs^2/mm [34]. β is the propagation constant, which could be calculated as $\beta = \omega n_{eff}/c$, where n_{eff} is the effective refractive index of a certain mode at the frequency of interest. ω_1 is the frequency of the anti-Stokes light, and ω_4 is the frequency of the Stokes light. ω_2 and ω_3 are the frequencies of two other transverse modes in the signal light. Considering the narrow bandwidth of seed light (the full width at half-maximum is about 0.18 nm) [28], it is assumed

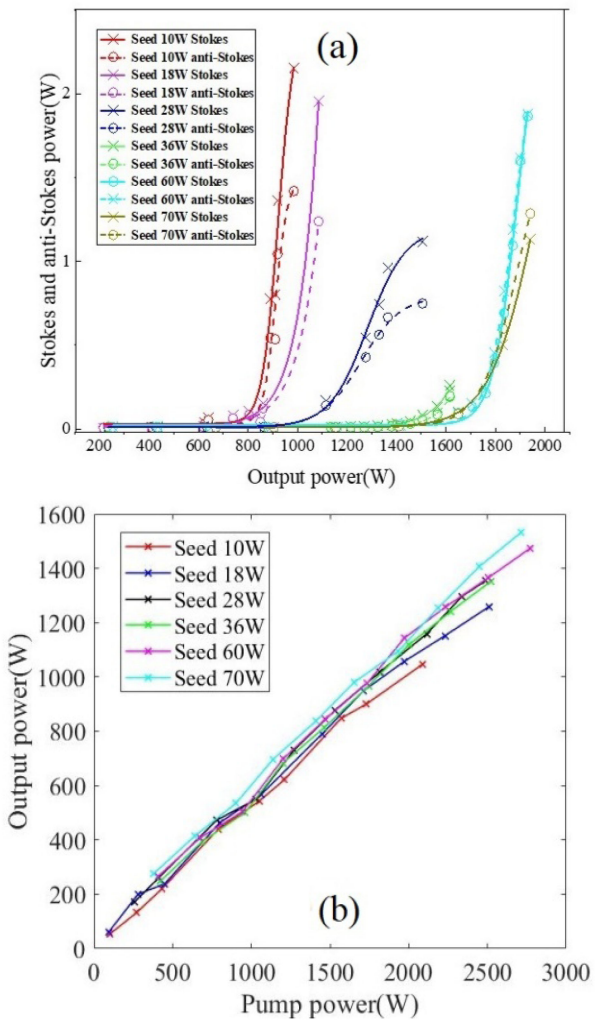

Fig. 3. (a) IM-FWM power versus total output power under different seed power; (b) Output power versus pump power under different seed power [29].

that $\omega_2 \approx \omega_3$. Then, the frequency shift $\Delta\omega$ should satisfy the relation $\Delta\omega = (\omega_1 - \omega_2) = (\omega_3 - \omega_4)$. Because the normalized frequency of the active core (i.e., Core 2 shown in Fig. 1) is about 3.9, LP_{01}, LP_{11} and LP_{21} modes can be supported in the active core. Thus, four cases of possible IM-FWM mode combinations are considered, which are given as (2):

$$\begin{aligned}
&\omega_2\left(LP_{01}\right)+\omega_3\left(LP_{11}\right)\rightarrow\omega_1\left(LP_{01}\right)+\omega_4\left(LP_{11}\right)\\
&------\text{Case } I\\
&\omega_2\left(LP_{01}\right)+\omega_3\left(LP_{11}\right)\rightarrow\omega_1\left(LP_{11}\right)+\omega_4\left(LP_{01}\right)\\
&------\text{Case } II\\
&\omega_2\left(LP_{01}\right)+\omega_3\left(LP_{21}\right)\rightarrow\omega_1\left(LP_{01}\right)+\omega_4\left(LP_{21}\right)\\
&------\text{Case } III\\
&\omega_2\left(LP_{01}\right)+\omega_3\left(LP_{21}\right)\rightarrow\omega_1\left(LP_{21}\right)+\omega_4\left(LP_{01}\right)\\
&------\text{Case } IV
\end{aligned} \tag{2}$$

It is necessary to mention that, since our seed light has a near diffractive beam with the beam quality (M^2 factor) around 1.08, the high order modes are assumed to be much weaker compared

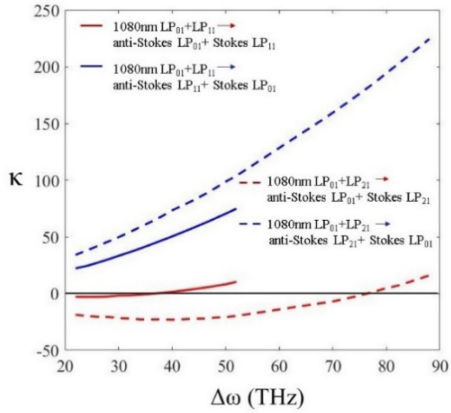

Fig. 4. The phase-mismatch κ versus the frequency shift $\Delta\omega$ under four possible IM-FWM mode combinations.

to the fundamental LP_{01} mode. Thus, the combinations which consider the interaction between the LP_{11} and LP_{21} modes in the signal light are neglected. Then, the phase mismatch as function of the frequency shift $\Delta\omega$ under the four cases is plotted in Fig. 4. The propagation constant β is calculated by a finite element analysis algorithm [38]. It is observed that the phase-matching condition of the IM-FWM is satisfied by Case I, when the frequency shift is $\Delta\omega = 36$ THz, and by Case III when the frequency shift is $\Delta\omega = 76$ THz. Since the signal wavelength is 1080 nm, the wavelengths of the anti-Stokes and Stokes in Case I should be 1057.8 nm and 1101.8 nm, respectively, while these wavelengths in Case III should be 1036.6 nm and 1124.8 nm, respectively.

Comparing the results to Fig. 2, it can be found that the wavelengths of the anti-Stokes and Stokes lights in Case I agree very well with the experimental observation (i.e., the two side lobes at 1058 nm and 1102 nm). Therefore, it can be concluded that the IM-FWM effect in our experiment is induced by the interaction of the 1080-nm LP_{01} and 1080-nm LP_{11} modes. Interestingly, there is still a small peak in Fig. 2(a), centered around 1040 nm, which is also in good agreement with the anti-Stokes wavelength of Case III. This means that the small peak around the1040 nm wavelength in Fig. 2(a) is induced by the IM-FWM effect, involving the 1036.6-nm LP_{01} and the 1124.8-nm LP_{21} modes. Apart from that, Fig. 2 implies that the IM-FWM of Case I should be much stronger than the one of Case III. Therefore, we will only consider the IM-FWM of Case I in the numerical study.

IV. Numerical Modal

With the transverse modes being determined in the previous section, the numerical study will be conducted. According to our knowledge, currently, there is no suitable numerical model to study the IM-FWM in the distributed side-pumped fiber amplifier. Let us first set the numerical model up. Considering that the IM-FWM effect is induced by various transverse modes, the mode competition, along with the transverse spatial-hole burning (TSHB) must be included in the model [35]. Besides, the special structure of the DSCCP fiber should also be considered. Therefore, we construct the numerical model by introducing the

TSHB and the IM-FWM into the rate-equation model of the DSCCP fiber amplifier given in [36]–[37] which is

$$\frac{dP^{\pm}_{\mathrm{pump1}}(z)}{dz} = \mp\gamma_1 P^{\pm}_{pump1}(z) \pm \gamma_2 P^{\pm}_{pump2}(z) \tag{4}$$

$$\begin{aligned}\frac{dP^{\pm}_{\mathrm{pump2}}(z)}{dz} = {} & \pm\Big[\sigma_{ep}P^{\pm}_{\mathrm{pump2}}(z) \\ & \times\int_0^{2\pi}\int_0^{r_{core}}\frac{n_2(r,\varphi,z)\,r}{(r_{clad})^2}drd\varphi - \sigma_{ap}P^{\pm}_{\mathrm{pump2}}(z) \\ & \times\int_0^{2\pi}\int_0^{r_{core}}\frac{n_1(r,\varphi,z)\,r}{(r_{clad})^2}drd\varphi \\ & + \gamma_1 P^{\pm}_{\mathrm{pump1}}(z) - \gamma_2 P^{\pm}_{\mathrm{pump2}}(z)\Big]\end{aligned} \tag{5}$$

$$\begin{aligned}\frac{dP_i(z)}{dz} = {} & \sigma_e\left[P_i(z) + 2h\frac{c^2}{\lambda_i^3}\Delta\lambda\right] \\ & \times\int_0^{2\pi}\int_0^{r_{core}} I_i(r,\varphi)\,n_2(r,\varphi,z)\,rdrd\varphi - \sigma_a P_i(z) \\ & \times\int_0^{2\pi}\int_0^{r_{core}} I_s(r,\varphi)\,n_1(r,\varphi,z)\,rdrd \\ & \varphi \pm C_i\Big(\prod_{k=1,2,3,4} P_k(z)\Big)^{1/2}\end{aligned} \tag{6}$$

Equation (3), shown at the bottom of this page, depicts the upper-level ions density distribution. $n_2(r, \varphi, z)$ is the upper-level ions density at the position (r, φ, z) and n_t (r, φ, z) is the total rare-earth ions density at the position (r, φ, z). P_i denotes the power for i[th] mode field involved in the IM-FWM, i.e., the 1058 nm LP_{01} mode (i = 1), the 1080 nm LP_{01} mode (i = 2), the 1080 nm LP_{11} mode (i = 3), and the 1102 nm LP_{11} mode (i = 4). I_i (r, Φ) is the normalized intensity profile of i[th] mode, which is calculated by a finite element analysis algorithm [38]. $\sigma_\alpha(\lambda_i)$, and $\sigma_e(\lambda_i)$ are the absorption and emission cross sections at the wavelength λ_i of the i[th] mode, while $\sigma_{\alpha p}$ and σ_{ep} are the absorption and emission cross sections at the pump wavelength, respectively.

Equations (4)–(5) depict the pump power evolution in the Core 1 and Cladding 3 respectively, which portrays the pump coupling process. $P^{\pm}_{\mathrm{pump1}}$ is the power pump in the core of the pump fiber (i.e., Core 1), while $P^{\pm}_{\mathrm{pump2}}$ is the pump power in the inner cladding of a signal fiber (i.e., Cladding 3, see Fig. 1). The "+" and "-" superscripts denote the forward and backward propagation, respectively. γ_1 and γ_2 are the coupling coefficients of the pump light between Cladding 3 and Core 1

TABLE II
PARAMETER VAULES USED IN THE CALCULATION

Parameters	Value	Parameters	Value
Core diameter (μm)	25	n_t (m^{-3})	1.0×10^{25}
Cladding diameter(μm)	250	γ_1, γ_2(m^{-1})	2
Core numerical aperture NA	0.065	σ_a	[40]
Core index	1.46	σ_e	[40]

[39]. In this paper, their values (see Table II) were adopted to make the numerical prediction of output power and efficiency agree well with the experimental results (see Figs. 3b and 5a). r_{core} is the radius of active fiber (i.e., Core 2).

Equation (6) depicts the power evolutions of the i[th] mode field involved in the IM-FWM, and C_i is the pertinent coupling coefficient of i[th] mode which is given by

$$C_i = 4\delta\kappa_i \sin[\Delta\varphi(z)]\iint\prod_{k=1}^{4}\sqrt{I_k(r,\varphi)}\,rdrd\varphi \tag{7}$$

The IM-FWM effect makes the 1080-nm signal power to be transferred to the 1058-nm anti-Stokes and 1102-nm Stokes light. Thus, the "+" sign in (6), is adopted for the 1058-nm LP_{01} and the 1102-nm LP11 modes. The "-" sign is used for the 1080-nm LP_{01} and the LP_{11} mode. δ is the nonlinear index coefficient (about 2.7×10^{-20} m^2/W) [34] and sin [$\Delta\Phi$(z)] corresponds to the phase matching effect. k_i is the value of wave vector of i[th] field in vacuum, which could be calculated by ω_i/c. The term $2h\frac{c^2}{\lambda_i^3}\Delta\lambda$, in the right side of (6), depicts the spontaneous emission (SE) contribution. $\Delta\lambda$ is the bandwidth of the four mode fields involved in the IM-FWM and is taken equal to 1 nm in our calculations. It should be noted that only when the phase matching condition is met the 1058-nm Stokes and 1102-nm anti-Stokes lights can be significantly amplified by the IM-FWM. Therefore, in the power amplification process, it is assumed that these four mode fields are well phase-matched, and thus sin [$\Delta\Phi$(z)] is equal to 1.

According to the experimental setup, two sub-amplifiers with the same length of the DSCCP fibers, are used in the distributed-pumped fiber amplifier. It is assumed that the length of the DSCCP fiber is L in each sub-amplifier. Then, the boundary conditions for the amplifier can be written as,

$$\begin{aligned} P_{1,4}(0) = 1\times10^{-5},\ P_2(0) = P_{seed}\,\eta \\ P_3(0) = P_{seed}\,(1-\eta) \\ P^{+}_{pump1}(0) = P^{-}_{pump1}(L) = \\ P^{+}_{pump1}(L) = P^{-}_{pump1}(2L) = P_p \end{aligned} \tag{8}$$

$$n_2(r,\varphi,z) = n_t(r,\varphi)\times\frac{\sum P_i(z)\,I_i(r,\varphi)\,\lambda_i\sigma_\alpha(i) + \sum P^{\pm}_{\mathrm{pump2}}(z)\,I_p\lambda_p\sigma_{\alpha p}}{\frac{hc}{\tau} + \sum P_i(z)\,I_i(r,\varphi)\,\lambda_i(\sigma_\alpha(i)+\sigma_e(i)) + \sum P^{\pm}_{\mathrm{pump2}}(z)\,I_p\lambda_p(\sigma_{\alpha p}+\sigma_{ep})} \tag{3}$$

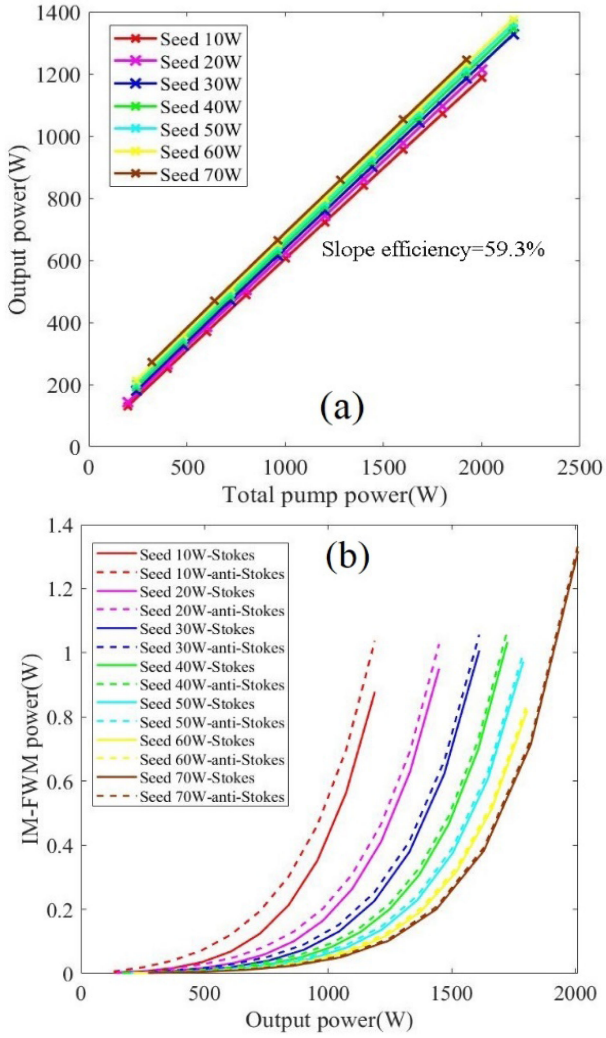

Fig. 5. (a) 1080-nm signal output power versus total pump power; (b) 1102-nm Stokes and 1058-nm anti-Stokes power versus total output power under different seed power.

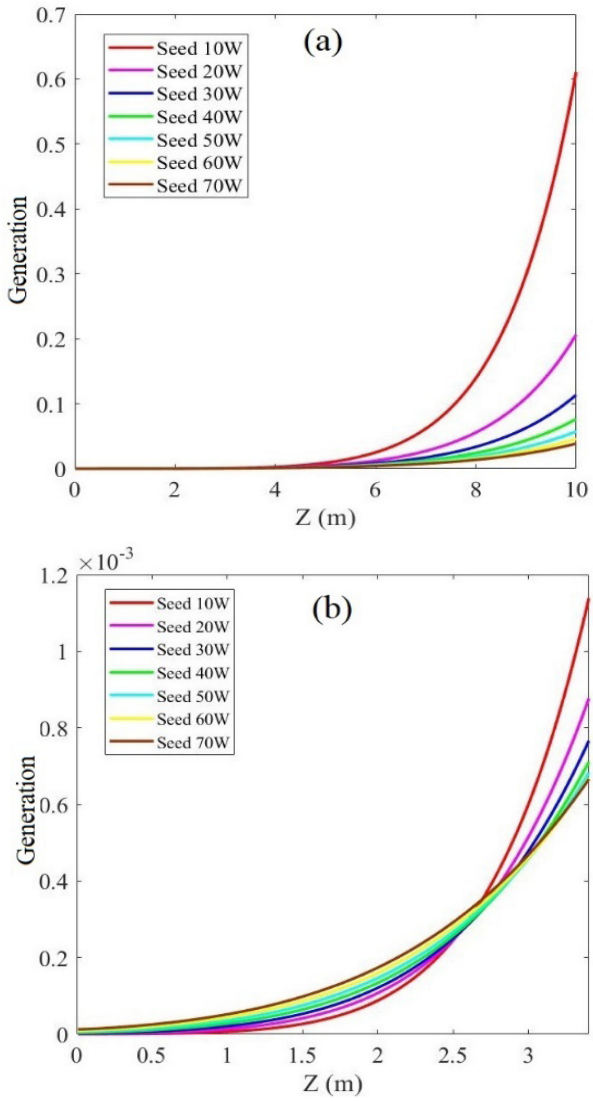

Fig. 6. (a) Generation along the fiber (0∼10 m); (b) generation along the fiber (0∼3.5 m).

where P_{seed} denotes the injected seed power and η is the proportion of the fundamental (i.e., LP_{01}) mode in the seed power. Here, it is also assumed that the splicing loss of the two sub-amplifiers should be negligible. Therefore, the i^{th} mode power input into the 2^{nd} sub-amplifier is equal to the i^{th} mode power output from the 1^{st} sub-amplifier. According to the experimental setup, the pump powers which injected into the four ports are assumed to be equal to P_p. Then, along with the boundary conditions, the model can be solved, providing the effect of IM-FWM on the output power P_i. For the numerical study it is firstly assumed that $\eta = 99\%$. This assumption is made based on two preconditions. The first one is that the seed source has a near diffractive-limit output (see [29]), meaning that the fundamental mode should take most of the seed light. Regarding the second, this value is chosen such that the numerical results of the slope efficiency and the Stokes and anti-Stokes powers will fit well with the experimental data, as seen in Fig. 3, Fig. 5, and Fig. 6. Besides, $P_{1,4}$ (0) is assumed to be 10^{-5} W, which is also chosen such that the numerical results fit well with the experimental data. Such an assumption is reasonable because the seed light contains unavoidable noise within the wavelengths of Stokes and anti-Stokes light.

V. Numerical Results and Discussions

Employing the aforementioned numerical model, the effect of seed light on the IM-FWM will be studied in this section. The parameter values used in the numerical calculation are given in Table II and are chosen in accordance with the experimental setup. Firstly, we calculate the output signal power (i.e., the total power including all the four modes) corresponding to various seed powers. The respective results are illustrated in Fig. 5(a). It can be found that the seed light has no obvious effect on the slope efficiency of the output power, which agrees with the experimental results shown in Fig. 3(b). Here, it should be noted that the SRS components must be significantly weaker compared to the signal power (see Fig. 2) in the experiment. Thus, the measured output power should be comparable with

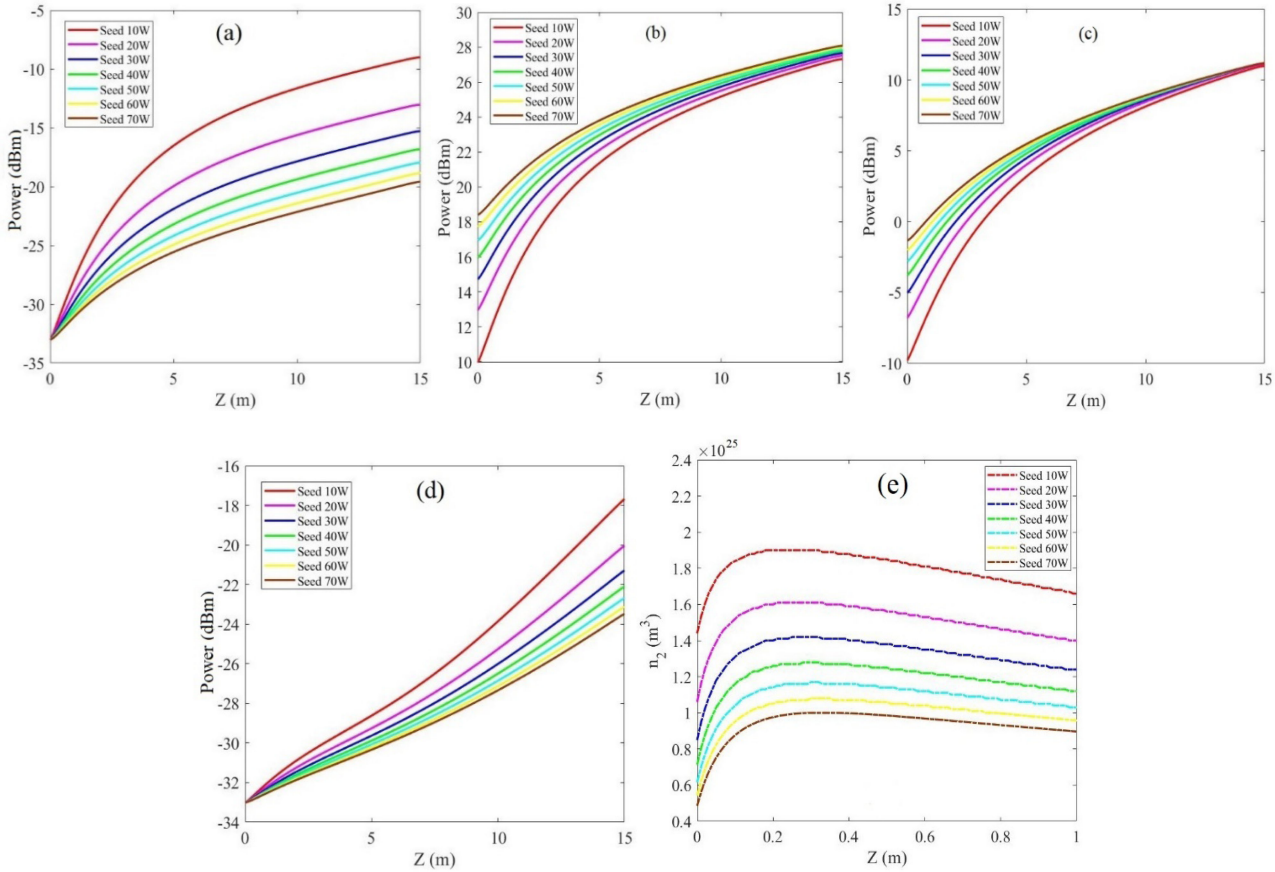

Fig. 7. Numerical results of variations of mode powers (a-d) and upper-level ions density (e) with the position z. (a) 1058-nm LP_{01} anti-Stokes; (b) 1080-nm LP_{01} signal light; (c) 1080-nm LP_{11} signal light; (d) 1102-nm LP_{11} Stokes light; (e) Upper-level ions density at the center of fiber cross section n_2 (00, z) variations under different seed power.

the numerical results, even though the SRS is neglected in the numerical model. Fig. 5(a) shows that the calculated slope efficiency is around 59.3%, very close to the experimental result which is around 53.8% and shown in Fig. 3(b).

Next, we calculate variations of the Stokes (i.e., the 1080 nm LP_{11} mode) and anti-Stokes (i.e., the 1080 nm LP_{01} mode) powers which correspond to various seed powers. The results are illustrated in Fig. 5(b). It can be seen that with each seed power, the anti-Stokes powers are slightly higher than their Stokes counterparts. From Fig. 2(e)–(f), it is obvious that this result is in good agreement with the experimental data, without the effect of SRS. It is implied that the 1058-nm LP_{01} mode (i.e., the anti-Stokes light) can receive more gain compared to the 1102-nm LP_{11} mode (i.e., the Stokes light). Furthermore, we find that the threshold of the IM-FWM is increased with the seed power. The latter, not only agrees well with our surprising experimental observations, but also suggests that these experimental observations are reasonable. In the numerical study, the IM-FWM threshold is defined as the output power when the Stokes power reaches 0.1% of the signal power.

To reveal the mechanism behind the seed effect on the IM-FWM threshold, the origin of the IM-FWM needs to be considered. As mentioned above, the IM-FWM is induced by the interaction of the four fields, i.e., the 1080-nm LP_{01} and LP_{11} modes, the 1058-nm LP_{01} mode, and the 1120-nm LP_{11} mode. Then, according to (6), two factors contribute to the gain of the IM-FWM; the Yb ions gain (i.e., the first two terms in right side of (6), and the nonlinear gain, which is determined by the production of the four mode powers (which is called "generation" in the next manuscript), as seen in the last terms of (6). Firstly, we examine the variation of the generation value along the fiber longitudinal position z because the strength of the IM-FWM can be directly determined by the nonlinear gain. The results are presented in Fig. 6.

Fig. 6(a) indicates that the generation value is obviously larger for a weaker seed power, when $z>5$ m. This enhances the nonlinear gain as well as the IM-FWM effect and it implies that a higher nonlinear gain is the origin of a stronger IM-FWM effect with weak seed light. Subsequently, we examined the variation of the generation value for a position $z<5$m, which is shown in Fig. 6(b). It was found that there is an intersection at the position z between the values 2.5m and 3.0m. When the position is smaller than 2.5m, the generation value is still larger with the higher seed power. This means that a stronger seed power will also lead to higher nonlinear gain of the IM-FWM at the beginning of signal light amplification. Such a case can be reversed only after the intersection. To reveal the reason of the reversion, the variations of the four modes power along the fiber are examined and presented in Fig. 7.

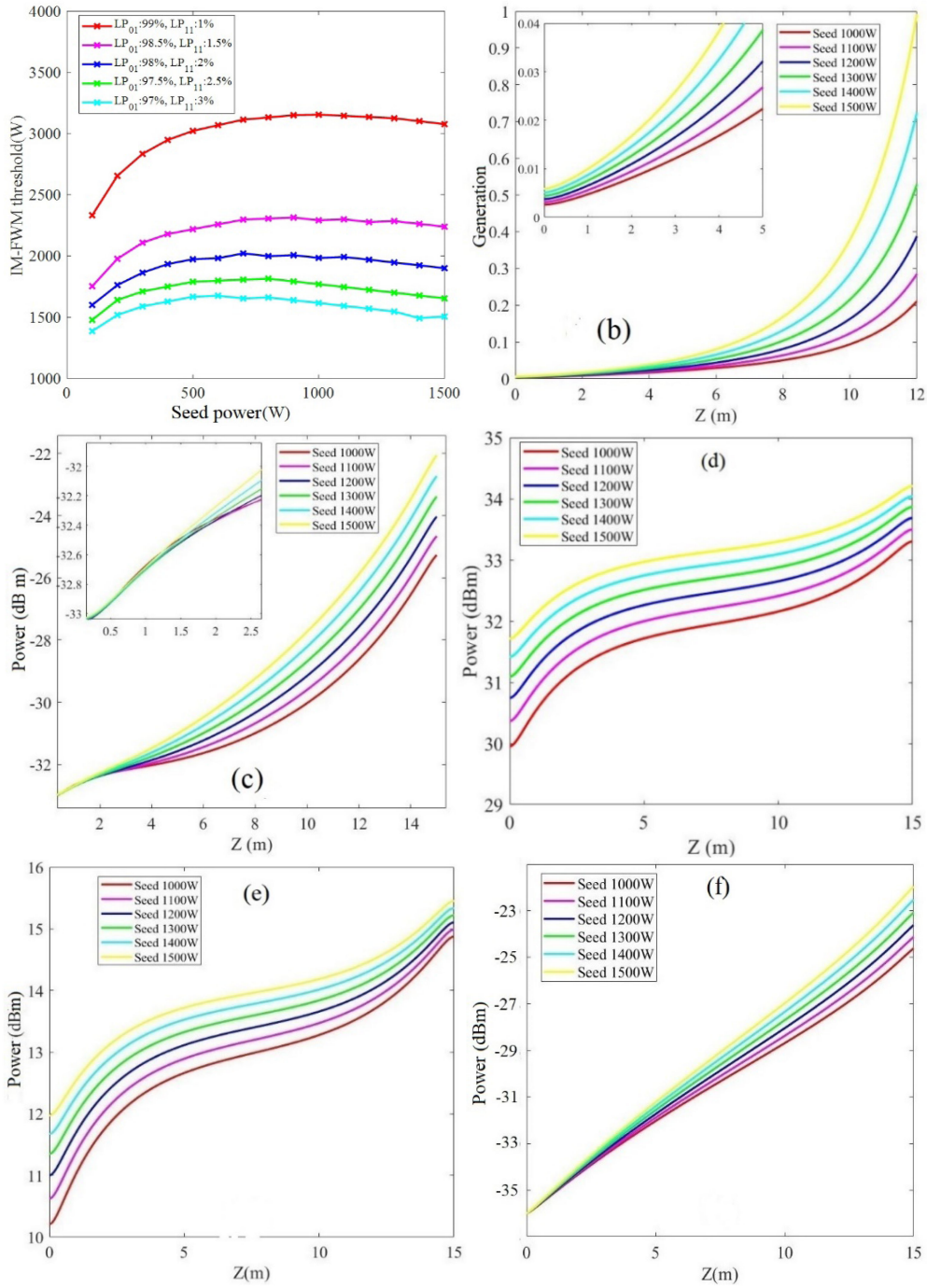

Fig. 8. (a) IM-FWM threshold versus the seed power under different mode proportions in the seed light; (b) generation along the fiber; (c) the variation of 1058-nm LP01 mode; (d) the variation of 1080-nm LP01 mode; (e) the variation of 1080-nm LP11 mode; (f) the variation of 1102-nm LP11 mode.

Fig. 7 indicates that there is no intersection of curves which correspond to various seed powers in each sub-figure, especially when the position z is z<5m. Moreover, from Fig. 7(b) and (c), it can be clearly seen that both the 1080-nm LP_{01} and LP_{11} modes obtain larger power as the seed power increases. Therefore, the intersection appearing in Fig. 6(b) is not induced by the power variations of the 1080-nm LP_{01} and LP_{11} modes. Fig. 7(a) and (d), depict that, although both the powers of the 1058-nm LP_{01} and 1102-nm LP_{11} modes increase with decreasing the seed power, the increment of 1058-nm LP_{01} mode is much faster than that of 1102-nm LP_{11} mode with the position being z<5m. Therefore, it can be concluded that the rapid increment of the 1058-nm LP_{01} mode is the origin of the intersection shown in Fig. 6(b) which, eventually, induces the stronger IM-FWM with the weaker seed light.

Following the above analysis, one question remains open, i.e., why does the power of the 1058-nm LP_{01} mode becomes larger with smaller seed power. This can be answered by considering

the effect of gain competition. Due to the similarity of the transverse mode profile, the 1058-nm LP_{01} and the 1080-nm LP_{01} modes should exhibit gain competition. In case the 1080-nm LP_{01} mode is not strong enough to fully extract the gain in the active fiber, the residual gain can be extracted by the 1058-nm LP_{01} mode and make the 1058-nm LP_{01} mode amplified. It should be noted that the 1080-nm LP_{01} mode takes the majority of seed power. Thus, the smaller the seed power, the less the 1080-nm LP_{01} mode, and the more gain is possible to be provided for the amplification of the 1058-nm LP_{01} mode. The increment of the 1058 nm LP_{01} mode power can be faster with smaller seed power. This can be verified with the upper-level ions density n_2 (00, z) of the upper-level ions, for peak intensity emerges at the center of the active fiber for LP_{01} mode, which is given in Fig. 7(e). It can be found that the value n_2 (00, z) increases monotonously with the decrement of seed power, which means that the gain abstraction should become less with the smaller seed power.

Up to this point and by employing numerical calculations, we have revealed the physics behind the experimental obsevation that the enhancement of the IM-FWM effect with the smaller seed power, i.e., the amplification of 1058-nm LP_{01} mode, emerges from the gain competition with the 1080-nm LP_{01} mode. However, it should be noted that in our analysis, the seed power was not larger than 70 W. It is still an open question how the the IM-FWM will vary with the seed power when this is further increased. To answer this question, the IM-FWM threshold with larger seed power is calculated and the results are shown in Fig. 8(a). It is found that the variation of IM-FWM threshold with the seed power is not monotonous. When the seed power is smaller than a certain value (e.g., 1000 W with the 1% LP_{11} mode in the seed light), the threshold increases monotonously with the seed power. However, when the seed power is larger than that value, the threshold decreases.

To further understand the numerical results, we have examined the variation of generation of the four mode powers, which is given in Fig. 8(b). It was found that the generation value increases monotonously with the increment of the seed power, and no intersection as the one in Fig. 6(b), appears. This, in turn, means that when the seed power is larger than 1000 W, more nonlinear gain is provided, rendering the IM-FWM stronger. The evolution of the four modes is illustrated in Fig. 8(c)–(f). Comparing Fig. 8(c) with Fig. 7(a), we find that the increment of the 1058-nm LP_{01} mode becomes much slower than the one given in Fig. 7(a). This means that when the seed power is larger than 1000 W the gain should be abstracted by the 1080-nm LP_{01} mode sufficiently enough, such that the 1058-nm LP_{01} mode will not be able to obtain sufficient gain from the Yb-ions. Then, the threshold will be mainly determined by the nonlinear gain and decreases by increasing the seed power instead.

In the previous study, the ratio of the 1080-nm LP_{11} mode in the seed light is set to be 1% and the reason has been stated in Section IV. However, how would the 1080-nm LP_{11} mode in the seed light influence the IM-FWM threshold is still a question. Thus, in Fig. 8(a), the effect of the ratio of the 1080-nm LP_{11} mode in the seed light is depicted. It can be found that the threshold of the IM-FWM is obviously increased by reducing the ratio of the 1080nm LP_{11} mode. The results are expected because, by reducing of the ratio, the power of 1080nm LP_{11} mode is lowered. This, in turn, lowers the nonlinear gain (determined by the generation of four mode powers) of the IM-FWM and the threshold of the IM-FWM increases. Fig. 8(a) also indicates that the optimum seed power will be also reduced, to some extent, by increasing the ratio of 1080nm LP_{11} mode.

VI. Conclusion

The influence of the seed power on the IM-FWM effect in a distributed side-pumped fiber amplifier 0is investigated for the first time, as far as we know. Our experiments reveal that the stronger IM-FWM effect emerges for a smaller seed power, while the IM-FWM threshold, with a 70 W seed power, can increase more than twice compared to the one which corresponds to 10W seed power. This observation contradicts our intuitive understanding that the IM-FWM effect should be enhanced by a larger signal power. To understand the experimental observation a numerical model is developed. The numerical results show that the IM-FWM effect can indeed be enhanced with the weaker seed power, being in good agreement with the experimental observation. It is also revealed that the IM-FWM enhancement with weaker seed should be induced by the gain competition between the 1080-LP_{01} and 1058-nm LP_{01} modes. A larger seed power, compared to the experimental case (70 W), is also considered in the numerical study and it is shown that there is an optimized seed power for the suppression of the IM-FWM effect. It is also found that the IM-FWM can be enhanced by increasing the LP_{11} mode in the seed light.

Here, it should be noted that the TMI (transverse modal instability) is not observed in the experimental process around the threshold of the IM-FWM. This means that the IM-FWM threshold should be smaller than the TMI threshold. In essence, the IM-FWM should not have an obvious effect on the beam quality of the fiber amplifier, as it cannot increase the total photon number of the LP_{11} mode. As shown in Case I in (2), one photon of the 1080-nm LP_{11} mode disappears and one photon of the 1102-nm LP_{11} mode is produced. In spite of that, the IM-FWM will lower the coherence of the signal light which is related to the TMI. However, how seriously the IM-FWM can affect the TMI is still not clear and requires further investigation.

The discussions in this work were based on the fiber structure given in Table II. It can be expected that the IM-FWM effect can be suppressed by increasing the dopant concentration which can shorten the active fiber length. Moreover, since the larger dopant concentration will result in higher gain, more residual gain can be provided for the amplification of 1058-nm LP_{01} mode, which would, to some extent, lead to the increase of the optimum seed power. Besides, the increase of the mode area of the active fiber should be beneficial with respect to the suppression of the IM-FWM effect. Our work can provide significant guidance for understanding the IM-FWM in high-power fiber lasers and amplifiers.

ACKNOWLEDGMENT

The authors would like to thank 23th Research institute of China electronic science and technology group for useful help in fabricating the DSCCP fiber. The authors also would like to express their gratitude to EditSprings (https://www.editsprings.cn/) for the expert linguistic services provided. The authors wish to thank the anonymous reviewers for their valuable suggestions.

REFERENCES

[1] F. Beier *et al.*, "Experimental investigations on the TMI thresholds of low-NA Yb-doped single-mode fibers," *Opt. Lett.*, vol. 43, no. 6, pp. 1291–1294, 2018.

[2] K. Shima, S. Ikoma, K. Uchiyama, Y. Takubo, M. Kashiwagi, and D. Tanaka, "5-kW single stage all-fiber Yb-doped single-mode fiber laser for materials processing," in *Proc. Fiber Lasers XV: Technol. Syst.*, 2018, Art. no. 105120C.

[3] M. Ackermann, G. Rehmann, R. Lange, U. Witte, and V. Krause, "Extraction of more than 10 kW from a single ytterbium-doped MM-fiber," in *Proc. Fiber Lasers XVI: Technol. Syst.*, 2019, Art. no. 1089717.

[4] H. Zhan, K. Peng, S. Liu, Y. Li, and Y. Wang, "Pump-gain integrated functional laser fiber towards 10 kW-level high-power applications," *Laser Phys. Lett.*, vol. 15, no. 9, 2018, Art. no. 095107.

[5] E. Stiles, "New developments in IPG fiber laser technology," in *Proc. 5th Int. Workshop Fiber Lasers*, 2009, Art. no. 370.

[6] C. Jauregui, J. Limpert, and A. Tünnermann, "High-power fiber lasers," *Nature Photon.*, vol. 7, no. 11, pp. 861–867, 2013.

[7] H. Zhan *et al.*, "5kW GTWave fiber amplifier directly pumped by commercial 976nm laser diodes," *Opt. Exp.*, vol. 24, no. 24, pp. 27087–27095, 2016.

[8] Y. Ye *et al.*, "Towards power improvement of all-fiber laser oscillators with 30 μm-core Yb-doped fibers by suppressing transverse mode instability," *Laser Phys. Lett.*, vol. 17, no. 8, 2020, Art. no. 085106.

[9] B. Yang *et al.*, "High power monolithic tapered ytterbium-doped fiber laser oscillator," *Opt. Exp.*, vol. 27, no. 5, pp. 7585–7592, 2019.

[10] Y. Ye *et al.*, "Industrial 6kW high-stability single-stage all-fiber laser oscillator based on conventional large mode area ytterbium-doped fiber," *Laser Phys.*, vol. 31, no. 3, 2021, Art. no. 035104.

[11] H. Jeff, "Fiber lasers ramp up the power," *Laser Focus World*, vol. 45, no. 12, pp. 53–57, 2009.

[12] J. W. Dawson *et al.*, "Analysis of the scalability of diffraction-limited fiber lasers and amplifiers to high average power," *Opt. Exp.*, vol. 16, no. 17, pp. 13240–13266, 2008.

[13] J. Cao, S. Guo, X. Xu, J. Chen, and Q. Lu, "Investigation on power scalability of diffraction-limited Yb-doped fiber lasers," *IEEE J. Sel. Topics Quantum Electron.*, vol. 20, no. 5, Sep./Oct. 2014, Art. no. 0903211.

[14] S. I. Kablukov, E. A. Zlobina, E.V. Podivilov, and S.A. Babin, "Output spectrum of Yb-doped fiber lasers," *Opt. Lett.*, vol. 37, no. 13, pp. 2508–2510, 2012.

[15] J. Zheng *et al.*, "Four-wave mixing effect on high-power continuous-wave all-fiber lasers," *Modern Phys. Lett. B*, vol. 32, no. 23, pp. 1850275, 2018, Art. no. 1850275.

[16] Y. Xiao, R. J. Essiambre, M. Desgroseilliers, A. M. Tulino, R. Ryf, and S. Mumta, "Theory of intermodal four-wave mixing with random linear mode coupling in few-mode fibers," *Opt. Exp.*, vol. 22, no. 26, pp. 32039–32059, 2014.

[17] R. Dupiol *et al.*, "Far-detuned cascaded intermodal four-wave mixing in a multimode fiber," *Opt. Lett.*, vol. 42, no. 7, pp. 1293–1296, 2017.

[18] G. Rademacher *et al.*, "Investigation of intermodal four-wave mixing for nonlinear signal processing in few-mode fibers," *IEEE Photon. Technol. Lett.*, vol. 30, no. 17, pp. 1527–1530, Sep. 2018.

[19] R. Essiambre *et al.*, "Experimental investigation of inter-modal four-wave mixing in few-mode fibers," *IEEE Photon. Technol. Lett.*, vol. 25, no. 6, pp. 539–542, Mar. 2013.

[20] T. Li, C. Zha, Y. Sun, M. Yi, W. Ke, and W. Peng, "3.5 kw bidirectionally pumped narrow-linewidth fiber amplifier seeded by white-noise-source phase-modulated laser," *Laser Phys.*, vol. 28, no. 10, 2018, Art. no. 105101.

[21] Z. Li *et al.*, "Experimental demonstration of transverse mode instability enhancement by a counter-pumped scheme in a 2 kw all-fiberized laser," *Photon. Res.*, vol. 5, no. 2, pp. 77–81, 2017.

[22] Q. Fang *et al.*, "5 kw near-diffraction-limited and 8 kw high-brightness monolithic continuous wave fiber lasers directly pumped by laser diodes," *IEEE Photon. J.*, vol. 9, no. 5, Oct. 2017, Art. no. 1506107.

[23] L. Yin, Z. Han, H. Shen, and R. Zhu, "Suppression of inter-modal four-wave mixing in high-power fiber lasers," *Opt. Exp.*, vol. 26, no. 12, pp. 15804–15818, 2018.

[24] Y. Wang, C.-Q. Xu, and H. Po, "Analysis of Raman and thermal effects in kilowatt fiber lasers," *Opt. Commun.*, vol. 242, no. 4-6, pp. 487–502, 2004.

[25] Y. Wang, C.-Q. Xu, and H. Po, "Thermal effects in kilowatt fiber lasers," *IEEE Photon. Technol. Lett.*, vol. 16, no. 1, pp. 63–65, Jan. 2004.

[26] H. Ying *et al.*, "2 kW pump-light-stripper-free distributed side-coupled cladding-pumped fiber oscillator," *Laser Phys. Lett.*, vol. 14, no. 6, 2017, Art. no. 065102.

[27] H. Chen *et al.*, "Experimental investigations on multi-kilowatt all-fiber distributed side-pumped oscillators," *Laser Phys.*, vol. 29, no. 7, 2019, Art. no. 075103.

[28] H. Chen *et al.*, "Experimental investigations on TMI and IM-FWM in distributed side pumped fiber amplifier," *IEEE Photon. J.*, vol. 12, no. 3, Jun. 2020, Art. no. 1502413.

[29] H. Chen *et al.*, "Weak-seed induced enhancement of stimulated Raman scattering in distributed side-pumped Yb-doped fiber amplifiers," *IEEE Photon. J.*, vol. 12, no. 6, Dec. 2020, Art. no. 7103412.

[30] K. H. Yla-Jarkko *et al.*, "Low-noise intelligent cladding-pumped L-band EDFA," *IEEE Photon. Technol. Lett.*, vol. 15, no. 7, pp. 909–911, Jul. 2003.

[31] N. M. Zervas, A. M. Zervas, and J. Kim, "Effective absorption in cladding-pumped fibers," in *Proc. SPIE - Int. Soc. for Opt. Eng.*, 2011, pp. 1–13.

[32] V. P. Gapontsev, V. Fomin, and N. Platonov, "Powerful fiber laser system," U.S. Patent 20,090,092,157A1, Sep. 2009.

[33] M. A. Mel'Kumov, I. Bufetov, M. M. Bubnov, A. V. Shubin, and E. M. Dianov, "Pump radiation distribution in multi-element first cladding laser fibres," *Quantum Electron.*, vol. 35, no. 11, pp. 996–1002, 2005.

[34] G. P. Agrawal, *Nonlinear Fiber Optics*. Amsterdam, The Netherlands: Elsevier, 2007.

[35] Z. Jiang and J. R. Marciante, "Impact of transverse spatial-hole burning on beam quality in large-mode-area Yb-doped fibers," *J. Opt. Soc. Amer. B*, vol. 25, no. 2, pp. 247–254, 2008.

[36] Z. Huang, J. Cao, S. Guo, J. Chen, and X. Xu, "Comparison of fiber lasers based on distributed side-coupled cladding-pumped fibers and double-cladding fibers," *Appl. Opt.*, vol. 53, no. 10, pp. 2187–2195, 2014.

[37] Z. Huang, J. Cao, S. Guo, J. Chen, X. Xu, and J. Leng, "Model of distributed side-coupled cladding-pumped fiber lasers," in *Proc. 28th Adv. Solid-State Lasers*, 2013, Art. no. ATu3A.27.

[38] F. Poli, A. Cucinotta, and S. Selleri, "Photonic crystal fibers. Properties and applications," in *Springer Series in Material Science*. Amsterdam, The Netherlands: Springer, 2007.

[39] Z. Huang, J. Cao, S. Guo, J. Hou, and J. Chen, "The characteristics of pump light in side-coupled cladding-pumped fibers," *Opt. Fiber Technol.*, vol. 19, no. 4, pp. 293–297, 2013.

[40] R. Paschotta, J. Nilsson, A. C. Tropper, and D. C. Hanna, "Ytterbium-doped fiber amplifiers," *IEEE J. Quantum Electron.*, vol. 33, no. 7, pp. 1049–1056, Jul. 1997.